J|A|C|S
ARTICLES
Published on Web 12/06/2002

Single Crystal EPR Studies of the Reduced Active Site of [NiFe] Hydrogenase from *Desulfovibrio vulgaris* Miyazaki F

Stefanie Foerster,[†] Matthias Stein,[†] Marc Brecht,[†] Hideaki Ogata,[‡] Yoshiki Higuchi,[‡,||] and Wolfgang Lubitz*[,§]

Contribution from the Max-Volmer-Laboratorium für Biophysikalische Chemie, Fakultät für Mathematik und Naturwissenschaften, Technische Universität Berlin, D-10623 Berlin, Germany, Division of Chemistry, Graduate School of Science Kyoto University, Sakyo-Ku, Kyoto 606-1, Japan and Max-Planck-Institut für Strahlenchemie, P.O. Box 10 13 65, D-45413 Mülheim an der Ruhr, Germany

Received July 1, 2002

Abstract: In the catalytic cycle of [NiFe] hydrogenase the paramagnetic Ni−C intermediate is of key importance, since it is believed to carry the substrate hydrogen, albeit in a yet unknown geometry. Upon illumination at low temperatures, Ni−C is converted to the so-called Ni−L state with markedly different spectroscopic parameters. It is suspected that Ni−L has lost the "substrate hydrogen". In this work, both paramagnetic states have been generated in single crystals obtained from the [NiFe] hydrogenase from *Desulfovibrio vulgaris* Miyazaki F. Evaluation of the orientation dependent spectra yielded the magnitudes of the *g* tensors and their orientations in the crystal axes system for both Ni−C and Ni−L. The *g* tensors could further be related to the atomic structure by comparison with the X-ray crystallographic structure of the reduced enzyme. Although the *g* tensor magnitudes of Ni−C and Ni−L are quite different, the orientations of the resulting *g* tensors are very similar but differ from those obtained earlier for Ni−A and Ni−B (Trofanchuk et al. *J. Biol. Inorg. Chem.* **2000**, *5,* 36−44). The *g* tensors were also calculated by density functional theory (DFT) methods using various structural models of the active site. The calculated *g* tensor of Ni−C is, concerning magnitudes and orientation, in good agreement with the experimental one for a formal Ni(III) oxidation state with a hydride (H^-) bridge between the Ni and the Fe atom. Satisfying agreement is obtained for the Ni−L state when a formal Ni(I) oxidation state is assumed for this species with a proton (H^+) removed from the bridge between the nickel and the iron atom.

Introduction

Hydrogenases catalyze the reversible oxidation of molecular hydrogen and play a vital role in anaerobic metabolisms of a wide variety of microorganisms. In many anaerobes that use H_2 as a source of energy, hydrogenases couple H_2 oxidation to the reduction of electron acceptors such as carbon dioxide, sulfate, or sulfur.[1] The latter two possess a central function in the energy generating mechanisms of sulfate reducing bacteria of the genus *Desulfovibrio*.

Three different kinds of hydrogenases have been characterized that can be distinguished by their metal content: the nickel−iron ([NiFe]) hydrogenases[2] including the subfamily of the nickel−iron−selenium ([NiFeSe]) hydrogenases,[3] the iron ([Fe]) hydrogenases,[4] and the "metal-free" hydrogenases.[5] Among those, [NiFe] hydrogenases represent the largest class.

The standard [NiFe] hydrogenase comprises a large conserved subunit (60 kDa), which contains the active site, and a small subunit harboring three iron−sulfur clusters.[2,6] X-ray crystallographic studies of the oxidized enzyme from *Desulfovibrio* (*D.*) *gigas*,[7] *D. vulgaris*,[8] *D. fructosovorans*,[9] and *D. desulfuricans* ATCC 27774[10] have revealed details of the heterobimetallic catalytic center (Figure 1). The Ni atom is coordinated by the sulfur atoms of four cysteine residues. Two of them act as a bridge between the metals, and two of them are bound to Ni as terminal cysteines. The X-ray structure indicated that the iron is further ligated by three inorganic diatomic ligands.[7−10]

* To whom correspondence should be addressed. Telephone: +49-208-306-3614,-3611. Fax: +49-208-306-3955. E-mail: lubitz@mpi-muelheim.mpg.de.
[†] Technische Universität Berlin.
[‡] Graduate School of Science Kyoto University.
[§] Max-Planck-Institut für Strahlenchemie.
[||] Present address: Department of Life Science, Graduate School of Science, Himeji Institute of Technology, 3-2-1 Koto Kamigori-cho, Akogun Hyogo, Japan.

(1) Thauer, R. K.; Jungermann, K.; Decker, K. *Bacteriol. Rev.* **1977**, *41*, 100−180.
(2) Albracht, S. P. J. *Biochim. Biophys. Acta* **1994**, *1188*, 167−204.
(3) Sorgenfrei, O.; Lindner, D.; Karas, M.; Klein, A. *Eur. J. Biochem.* **1993**, *213*, 1355−1358.
(4) Adams M. W. W. *Biochim. Biophys. Acta* **1990**, *1020*, 115−145.
(5) Thauer, R. K.; Klein, A. R.; Hartmann, G. C. *Chem. Rev.* **1996**, *96*, 3031−3042.
(6) Vignais, P. M.; Billoud, B.; Meyer, J. *FEMS Microbiol. Rev.* **2001**, *25*, 455−501.
(7) Volbeda, A.; Charon, M. H.; Piras, C.; Hatchikian, E. C.; Frey, M.; Fontecilla-Camps, J. C. *Nature* **1995**, *373*, 580−587.
(8) Higuchi, Y.; Yagi, T.; Yasuoka, N. *Structure* **1997**, *5*, 1671−1680.
(9) Rousset, M.; Montet, Y.; Guigliarelli, B.; Forget, A.; Asso, M.; Bertrand, P.; Fontecilla-Camps, J. C.; Hatchikian, E. C. *Proc. Natl. Acad. Sci. U.S.A.* **1998**, *95*, 11625−11630.
(10) Matias, P. M.; Soares, C. M.; Saraiva, L. M.; Coelho, R.; Morais, J.; Le Gall, J.; Carrondo, M. A. *J. Biol. Inorg. Chem.* **2001**, *6*, 63−81.

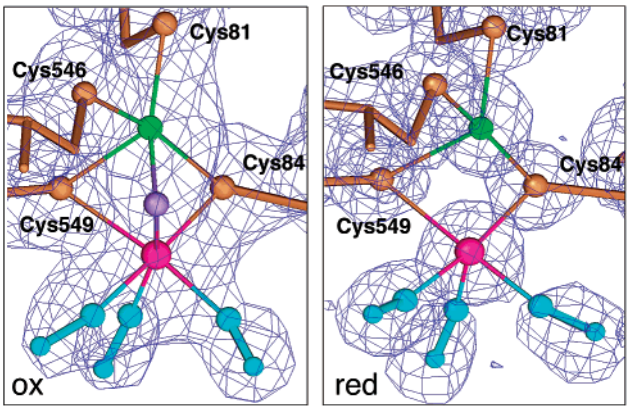

Figure 1. $2F_o-F_c$ electron density map and atomic structure of the active site of *D. vulgaris* Miyazaki F as obtained from X-ray structure analysis. (Ni: green. Fe: pink. Cys: yellow. Diatomics: blue. Bridge: violet.) Left: The oxidized state[8] results from a mixture of the Ni−A, the Ni−B, and probably the oxidized EPR silent state Ni−Si. Right: The reduced state (probably a mixture of Ni−C and Ni−R),[13] the third bridging ligand is lost upon reduction.

They have been identified by FTIR spectroscopy as one CO and two CN^- for the hydrogenases from *Allochromatium* (*A.*) *vinosum* and *D. gigas*.[11,12] On the basis of X-ray structure and mass spectrometric analysis, one SO, one CO, and/or CN^- have been proposed for the hydrogenase from *D. vulgaris* Miyazaki F;[8,13,14] however, FTIR spectroscopic investigations revealed only the presence of CN^- and CO.[14]

In the as-isolated, that is, oxidized enzyme, a third bridging ligand between the nickel and the iron atom was found whose chemical nature is still a matter of debate. The small ligand may be either an oxygen, as discussed in refs 15 and 16, or a sulfur species.[8,10] The latter assignment is based on the long ligand−metal distance, the bond angle of only 97°, and the temperature factor that attains a reasonable value when sulfur is taken for the structure refinement.[8,10] The coordination geometry of the nickel ion in the oxidized state can best be described as a slightly distorted octahedron with one unoccupied ligand position. In the reduced enzyme, the bridging ligand is absent in the X-ray structure[13] (see Figure 1).

During catalysis, the hydrogenase cycles through various redox states and several of them are paramagnetic. These are termed Ni−A, Ni−B, and Ni−C. In aerobic enzyme preparations, a mixture of the paramagnetic "ready" (for Ni−B, g tensor principal values are 2.33, 2.16, and 2.01) and "unready" (for Ni−A, $g_i \approx 2.31, 2.24, 2.01$) forms is found, differing in their activation rate.[2] Ni−B is easily activated by hydrogen within a few minutes, whereas Ni−A needs longer incubation times, up to a few hours. In reductively activated enzymes, an EPR detectable species is obtained, denominated Ni−C ($g_i \approx 2.19, 2.14, 2.01$).[2] Upon illumination of the Ni−C state, a new species, called Ni−L, is generated (for Ni−L, $g_i \approx 2.29, 2.11, 2.05$).[2] It is stable at temperatures below 100 K. At higher temperatures, a conversion back to Ni−C is observed.[2] The EPR properties of Ni−L are different from those of the other forms; in particular, the smallest g tensor component is shifted from $g_3 \approx 2.01$ to $g_3 \approx 2.05$.

Upon further reduction of the enzyme, the iron−sulfur clusters are reduced. The proximal $[4Fe-4S]^+$ cluster ($S = {}^1/_2$) magnetically interacts with the unpaired spin at the [NiFe] center in both forms, Ni−C and Ni−L. This interaction leads to a splitting of the EPR lines detectable below 10−15 K (termed "split" Ni−C or Ni−L).[17,18] At higher temperature, this interaction is not seen in the spectra because of increased relaxation rates of the iron−sulfur clusters.[19]

Investigations and analyses of the EPR spectra of ^{61}Ni-substituted hydrogenase indicated that the Ni atom bears the main part of the spin density of the active site in the oxidized as well as in the H_2 reduced states.[20−22] ENDOR measurements on an ^{57}Fe-substituted sample[23] revealed that only a vanishingly small part of the spin is found at the iron atom in all states. Thus, the [NiFe] center of hydrogenases can safely be assumed to be a bimetallic cluster with an iron atom in the low spin Fe(II) ($S = 0$) state. The oxidation and spin state of Ni is, however, less clear.

The active sites of [NiFe] hydrogenases are transition metal clusters with four cysteines being "noninnocent" ligands. They are capable of delocalizing metal d electrons and consequently may carry significant amounts of unpaired spin density.[24,25] Thus, the model of clearly defined oxidation states, as commonly applied in chemistry, should be used with care. In the following, the oxidation states of Ni will be addressed as *formal* oxidation states to emphasize whether a formal reduction or oxidation has taken place, leading to a new paramagnetic state. Recently, it has been shown that density functional theory (DFT) calculations can accurately probe the electronic structure of bioinorganic complexes.[26,27] With the availability of an efficient and reliable treatment of scalar relativistic (SR) effects and spin−orbit (SO) couplings in the ZORA Hamiltonian,[28] one can calculate magnetic resonance parameters, that is, g, electron−nuclear hyperfine, and electric quadrupole coupling tensors, directly from a Kohn−Sham wave function. We have demonstrated the accuracy of this method for several transition metal

(11) Happe, R. P.; Roseboom, W.; Pierik, A. J.; Albracht, S. P. J.; Bagley, K. A. *Nature* **1997**, *385*, 126.
(12) de Lacey, A. L.; Hatchikian, E. C.; Volbeda, A.; Frey, M.; Fontecilla-Camps, J. C.; Fernandez, V. M. *J. Am. Chem. Soc.* **1997**, *119*, 7181−7189.
(13) Higuchi, Y.; Ogata, H.; Miki, K.; Yasuoka, N.; Yagi, T. *Structure* **1999**, *7*, 549−556.
(14) Higuchi, Y.; Toujou, F.; Tsukamoto, K.; Yagi, T. *J. Inorg. Biochem.* **2000**, *80*, 205−211.
(15) Volbeda, A.; Garcin, E.; Piras, C.; de Lacey, A. L.; Fernandez, V. M.; Hatchikian, E. C.; Frey, M.; Fontecilla-Camps, J.-C. *J. Am. Chem. Soc.* **1996**, *118*, 12989−12996.
(16) Stein, M.; van Lenthe, E.; Baerends, E. J.; Lubitz, W. *J. Am. Chem. Soc.* **2001**, *123*, 5839−5840.
(17) Cammack, R.; Patil, D. S.; Fernandez, V. M. *Biochem. Soc. Trans.* **1985**, *13*, 572−578.
(18) Teixeira, M.; Moura, I.; Xavier, A. V.; Moura, J. J. G.; LeGall, J.; Der Vartanian, D.; Peck, H. D., Jr.; Huynh, B. H. *J. Biol. Chem.* **1989**, *264*, 16435−16450.
(19) Guigliarelli, B.; More, C.; Fournel, A.; Asso, M.; Hatchikian, E. C.; Williams, R.; Cammack, R.; Bertrand, P. *Biochemistry* **1995**, *34*, 4781−4790.
(20) Albracht, S. P. J.; Graf, E. G.; Thauer, R. K. *FEBS Lett.* **1982**, *140*, 311−313.
(21) Moura, J. J. G.; Moura, I.; Huynh, B. H.; Krüger, H. J.; Teixeira, M.; DuVarney, R. G.; DerVartanian, D. V.; Xavier, A. V.; Peck, H. D., Jr.; LeGall, J. *Biochem. Biophys. Res. Commun.* **1982**, *108*, 1388−1393.
(22) Krüger, H. J.; Huynh, B. H.; Ljungdahl, P. O.; Xavier, A. V.; Der Vartanian, D. V.; Moura, I.; Peck, H. D., Jr.; Teixeira, M.; Moura, J. J.; LeGall, J. *J. Biol. Chem.* **1982**, *24*, 14620−14623.
(23) Huyett, J. E.; Carepo, M.; Pamplona, A.; Franco, R.; Moura, I.; Moura, J. J. G.; Hoffman, B. M. *J. Am. Chem. Soc.* **1997**, *119*, 9291−9292.
(24) Coyle, C. I.; Stiefel, E. I. In *The Bioinorganic chemistry of nickel*; Lancaster, J. R., Jr., Ed.; VCH: New York, 1988; Chapter 1, pp 1−28.
(25) Stein, M.; Lubitz, W. *Phys. Chem. Chem. Phys.* **2001**, *3*, 2668−2675.
(26) Siegbahn, P. E. M.; Blomberg, M. R. A. *Chem. Rev.* **2000**, *100*, 421−438.
(27) Blomberg, M. R. A.; Siegbahn, P. E. M. *J. Phys. Chem. B* **2001**, *105*, 9375−9386.
(28) van Lenthe, E.; Wormer, P. E. S.; van der Avoird, A. *J. Chem. Phys.* **1997**, *107*, 2488−2498.

systems,[29,30] for evaluating g values and the spin populations of the paramagnetic states of [NiFe] hydrogenases[16,25] and for explaining the difference between [NiFe] and [NiFeSe] hydrogenases.[31] The method can thus be used to get insight into the electronic and geometrical structures of the intermediate states of the catalytic cycle of the hydrogenases by comparing calculated magnetic interaction tensors obtained from geometrically optimized models of the enzyme with tensors measured by EPR techniques.

EPR spectroscopic studies in frozen solutions yield, however, only the g tensor principal values.[32] A direct determination of the orientation of the principal axes of the g tensor with respect to the crystal structure, which can be related to the molecular structure, is available from EPR studies on single crystals. This has been demonstrated earlier by Geβner et al.[33] and Trofanchuk et al.[34] for the oxidized states of the enzyme using single crystals of the hydrogenase from *D. vulgaris* Miyazaki F.

In this work, we present the results of single-crystal EPR studies of the hydrogenase in the Ni−C and the Ni−L state. The availability of an X-ray structure at high resolution of the reduced hydrogenase from *D. vulgaris* Miyazaki F[13] allows us to relate the g tensor orientation of the Ni−C and Ni−L states to the molecular structure. Furthermore, we compare the derived experimental g tensor magnitudes and orientations with those proposed by density functional theory (DFT) calculations, performed on various geometrically optimized models of the active sites in the Ni−C and Ni−L form. The results are compared with the work of Müller et al.,[35] who determined the g tensor orientation for Ni−C based on EPR and ENDOR data on two different hydrogenases in frozen solution and obtained a different orientation. On the basis of our experimental and theoretical work, we will address several of the open questions in hydrogenase research, namely the formal oxidation states of nickel in all its paramagnetic intermediate states, the structure of the [NiFe] cluster, including the type of the third bridging ligand between the metals, and the functional role of the active center of the enzyme in the hydrogen conversion process.

Materials and Methods

Sample Preparation. The membrane-bound hydrogenase from *D. vulgaris* Miyazaki F was isolated and purified as described previously.[36] Single crystals of the hydrogenase were grown by the sitting drop vapor diffusion method from 33% MPD (2-methyl-2,4-pentane-diol) and 25 mM TrisHCl buffer solution at pH 7.4.[37] The crystals belong to the orthorhombic space group $P2_12_12_1$ and contain four magnetically inequivalent molecules (sites) per unit cell. Their respective orientations are related to each other by a 2_1 screw axis. The size of the crystals used for EPR experiments was approximately 1−2 mm × 0.5 mm × 0.5 mm. The methyl viologen soaked crystals (1 mM methyl viologen in the precipitant solution) were placed in thin walled quartz capillaries that were marked to indicate the initial position for the angular dependent EPR experiments. These capillaries were then transferred to quartz EPR tubes (Wilmad 707SQ, i.d. 3 mm, o.d. 4 mm or 705PQ, i.d. 2 mm, o.d. 3 mm). The orientation of the crystal axes relative to the laboratory axes system was determined by a preceding fit of the angular dependence of the EPR transitions of the oxidized crystals at room temperature by use of the known direction cosines of the g tensors of Ni−A and Ni−B (for details see ref 34). These crystals were then reduced under pure hydrogen gas at 37 °C and atmospheric pressure for 2−3 h. The position of the crystals in the tube was not changed during this procedure. The EPR spectra of the crystals were subsequently tested at room temperature. Ni−A/B EPR transitions disappeared, and a new set of signals belonging to Ni−C emerged. The crystals were then rapidly frozen in liquid nitrogen. Illumination of the crystals, to gain the Ni−L state, was performed with white light (halogen photo optic lamp, 250 W) at liquid nitrogen temperature (77 K).

Solutions of 2 M $NaClO_4$/HCl, pH = 1.5, with variable amounts of anhydrous $CuSO_4$ (100−500 μM) were used as a EPR standard for the spin quantification that was carried out as described in ref 38.

EPR Experiments and Data Analysis. EPR measurements on single crystals were performed at X-band with a Bruker ESP 300E spectrometer equipped with a Bruker dielectric ring resonator (ESP380-1052 DLQ-H) and an Oxford helium cryostat CF 935 (4−200 K). Enzyme solutions were measured in a Bruker double resonator (4105DR) equipped with an Oxford helium cryostat ESR 910. The field was calibrated with a Bruker ER035 teslameter, and the microwave frequency was measured with a Hewlett-Packard 5352B frequency counter. CW EPR spectra were recorded at $T = 298$ K and $T = 50$ K.

***g* Tensor Analysis.** The g tensor is characterized by three principal values: g_1, g_2, and g_3. The orientation of the principal axes with respect to the laboratory frame is obtained from analyzing the angular dependence of EPR transitions of single crystals. Experimentally, the respective spectral positions $g(\theta,\phi)$ are obtained from the resonance condition

$$h\nu = g(\theta,\phi)\beta B_0 \qquad (1)$$

where h is Planck's constant, ν is the spectrometer frequency, β is the Bohr magneton, and $g(\theta,\phi)$ is the effective g value. The angles θ and ϕ describe the orientation of the g tensor principal axes with respect to the magnetic field B_0. Depending on the number j of magnetically inequivalent molecules per unit cell (sites), we observe a corresponding number of resonance positions.[39] In the case of the space group $P2_12_12_1$, four magnetically distinct molecules are found in the unit cell; thus, one expects a maximum of four resonance lines in the EPR spectrum. If the magnetic field is located in a crystallographic plane, two signals pairwise coincide and a maximum of two signals is observed. If B_0 is parallel to one of the crystallographic axes, only one 4-fold degenerate resonance line is detected.

In our work, the g tensor principal axes have been determined by investigation of arbitrarily oriented single crystals. Three right-handed, orthogonal reference frames were defined: the laboratory frame (**L**), the crystal frame (**C**), and the intrinsic frame (**I**). In the latter, the g and g^2 tensors are diagonal and $i = 1, 2, 3$ represents the tensor principal axes. These three frames are related by rotations, which can be described by three Euler angles each. In our analysis, we determined the direction cosines of the g tensor principal axes (1, 2, 3) in the crystal frame (a, b, c). The fit routine always attributes the largest principal g value

(29) Stein, M. *Insight into the Mechanism of [NiFe] Hydrogenase by means of Magnetic Resonance Experiments and DFT Calculations*. Doctoral Thesis, Technische Universität Berlin, Berlin, Germany, 2001.
(30) Stein, M.; van Lenthe, E.; Baerends, E. J.; Lubitz, W. *J. Phys. Chem. A* **2001**, *105*, 416−425.
(31) Stein, M.; Lubitz, W. *Phys. Chem. Chem. Phys.* **2001**, *3*, 5115−5120.
(32) Moura, J. J. G.; Teixeira, M.; Moura, I.; LeGall, J. In *The Bioinorganic chemistry of nickel*; Lancaster, J. R., Jr., Ed.; VCH: New York and VCH Verlagsgesellschaft mbH: Weinheim, Germany, 1988; Chapter 9, pp 191−226.
(33) Geβner, C.; Trofanchuk, O.; Kawagoe, K.; Higuchi, Y.; Yasuoka, N.; Lubitz, W. *Chem. Phys. Lett.* **1996**, *256*, 518−524.
(34) Trofanchuk, O.; Stein, M.; Geβner, C.; Lendzian, F.; Higuchi, Y.; Lubitz, W. *J. Biol. Inorg. Chem.* **2000**, *5*, 36−44.
(35) Müller, A.; Tscherny, I.; Kappl, R.; Hatchikian, E. C.; Hüttermann, J.; Cammack, R. *J. Biol. Inorg. Chem.* **2002**, *7*, 177−194.
(36) Yagi, T.; Kimura, K.; Daidoji, H.; Sakai, F.; Tamura, S.; Inokuchi, H. *J. Biochem. (Tokyo)* **1976**, *79*, 661−671.
(37) Higuchi, Y.; Yasuoka, N.; Kakudo, M.; Katsube, Y.; Yagi, T.; Inokuchi, H. *J. Biol. Chem.* **1987**, *262*, 2823−2825.
(38) Weil, J. A.; Bolton, J. R.; Wertz, J. E. *Electron Paramagnetic Resonance;* Jon Wiley & Sons: New York, 1994.
(39) Morton, J. R.; Preston, K. F. *J. Magn. Reson.* **1983**, *52*, 457−474.

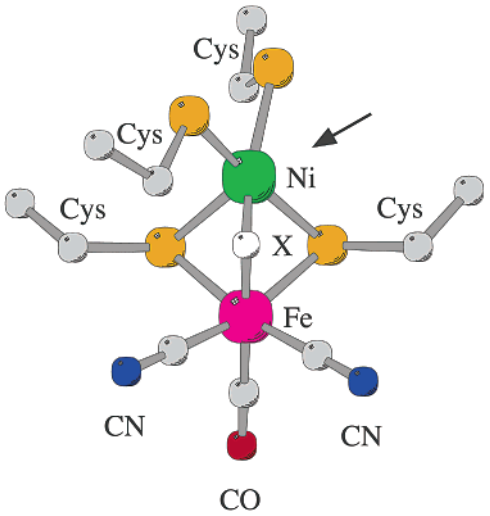

Figure 2. Composition of the model of the active site used for DFT calculations: X denotes the bridging ligand (in the reduced states a hydrogenic species or empty) and Cys denotes ethanethiolate residues as a model for the cysteines. The arrow points to the vacant axial sixth coordination site at the nickel. Note that the structure shown is the result of the geometry optimization for Ni−C with X = H^-. (Figures 2 and 6−8 were generated using the program MOLSCRIPT.[69])

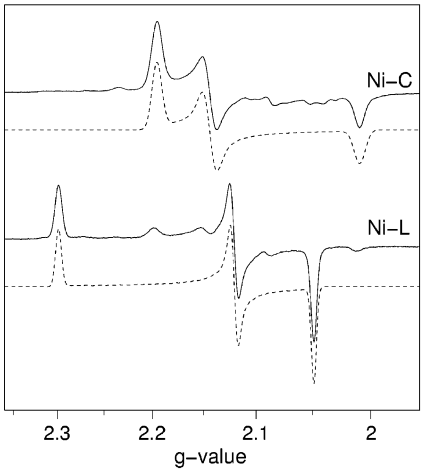

Figure 3. EPR spectra of reduced (Ni−C) and illuminated (Ni−L) solutions of the [NiFe] hydrogenase from *D. vulgaris* Miyazaki F and the respective simulations (dashed). The simulations were performed using an in-house simulation program[70] with the following parameters: g_i = 2.195, 2.144, 2.010 (error ± 0.002) and a line width of 1.1−1.3 mT (for Ni−C), g_i = 2.296, 2.118, 2.046 (error ± 0.002) and a line width of 0.4−0.6 mT (for Ni−L). Experimental conditions: X-Band, 9.6 GHz, T = 50 K, microwave power 1 mW, field modulation 100 kHz, modulation amplitude 1 mT, accumulation time 420 s, each.

to g_1 and the smallest to g_3. Detailed information about the fit algorithm used can be found in ref 33.

The effective g values of the four sites j, $g_j(\theta,\phi)$, were collected from EPR spectra of single crystals in an arbitrary orientation rotated about an axis perpendicular to the magnetic field by an angle α. By a simultaneous fit of all four sites using a numerical fit routine based on a simplex algorithm described in detail in ref 40, the three principal g values and the six Euler angles defining the relations between the frames **L** and **C** and between **C** and **I** have been determined.

DFT Calculations. We performed relativistic DFT calculations within the "zero-order regular approximation" (ZORA) for relativistic effects[41−43]. The ZORA formalism as implemented in the Amsterdam Density Functional (ADF) package was applied.[44,45] The calculations are single-point calculations at nonrelativistic (NR) or scalar-relativistic (SR) geometrically optimized structures, since no gradients for ZORA calculations with spin−orbit coupling are available.[43] For all calculations, we used the BP86 exchange-correlation functional[46−48] that has been shown to yield good results in calculating g tensors.[49] Geometries were optimized with an all-electron double-ζ Slater-type basis set with polarization functions (basis II in ADF nomenclature). A model cluster was constructed from the PDB coordinates of the enzyme (2FRV[15]). The model consists of a nickel, an iron atom, two CN^- and one CO as terminal ligands to the iron atom,[11] and four $^-S-CH_2-CH_3$ moieties representing the cysteine amino acids (Figure 2). Even though an SO is proposed as a terminal ligand to the iron in the active site of *D. vulgaris* Miyazaki F, it was not chosen as a ligand in the model, as spectroscopic properties such as g values could not be reproduced, see.[16,25,29] During the geometric optimizations, no constraints were imposed on the cluster.

Results and Discussion

EPR Measurements and Fit of the Data. Representative EPR spectra of Ni−C and Ni−L in frozen solutions are shown in Figure 3. The principal g values, g_1, g_2, and g_3, that are very similar to values measured for [NiFe] hydrogenases from other organisms[32] have been found by simulations (see Figure 3, caption).

For the determination of the g tensor principal axes with respect to the spatial structure of the active site, a knowledge of the orientation of the crystallographic axes (a, b, c) is required. In previous work of our group, the g tensor orientations of the states Ni−A and Ni−B with respect to a, b, and c have been determined by a combination of EPR spectroscopic and X-ray diffraction data.[33,34] By using these known g tensor parameters, we assigned the crystal axes orientation for our specifically mounted crystal in the oxidized state (Ni−A/B). Since the orientation of the crystal was not changed during activation and conversion to Ni−C, we related the orientation of the crystal axes of the oxidized to that of the reduced state. After illumination of the sample with white light, a partial conversion of Ni−C to Ni−L was achieved. This allowed us to measure the g tensor orientation relative to the crystal axes of both forms in the same crystal and in one set of angular dependent EPR spectra (Figure 4).

According to our EPR experiments, no major structural changes of the protein took place upon reduction and the single crystalline character of the sample was fully retained. Additional evidence for that came from X-ray structure analysis. The atomic coordinates hardly differed from those of the oxidized enzyme concerning the direct Ni coordination sphere. The rms (root-mean-square) deviation of the distances for atomic positions between the oxidized and reduced structure was 0.29 Å for the

(40) Geβner C. *NiFe−Hydrogenasen: Beiträge der EPR−Spektroskopie zur Strukturaufklärung des aktiven Zentrums*. Doctoral Thesis, Technische Universität Berlin, Berlin, Germany, 1996.
(41) van Lenthe, E.; Baerends, E. J.; Snijders, J. G. *J. Chem. Phys.* **1993**, *99*, 4597−4610.
(42) van Lenthe, E.; Baerends, E. J.; Snijders, J. G. *J. Chem. Phys.* **1994**, *101*, 9783−9792.
(43) van Lenthe, E.; Ehlers, A.; Baerends, E. J. *J. Chem. Phys.* **1999**, *110*, 8943−8953.
(44) *Scientific Computing and Modelling NV, ADF Program System*, release 2000.02; Vrije Universiteit, Theoretical Chemistry: De Boelelaan 1083, 1081 HV Amsterdam, The Netherlands.
(45) te Velde, G.; Bickelhaupt, F. M.; Baerends, E. J.; Fonseca-Guerra, C.; Van Gisbergen, S. J. A.; Snijders, J. G.; Ziegler, T. *J. Comput. Chem.* **2001**, *22*, 931−967.
(46) Becke, A. D. *Phys. Rev.* **1988**, *A38*, 3098−3100.
(47) Perdew, J. P. *Phys. Rev.* **1986**, *B33*, 8822−8824.
(48) Perdew, J. P. *Phys. Rev.* **1986**, *B34*, 7406.
(49) Belanzoni, P.; van Lenthe, E.; Baerends, E. J. *J. Chem. Phys.* **2001**, *114*, 4421−4433.

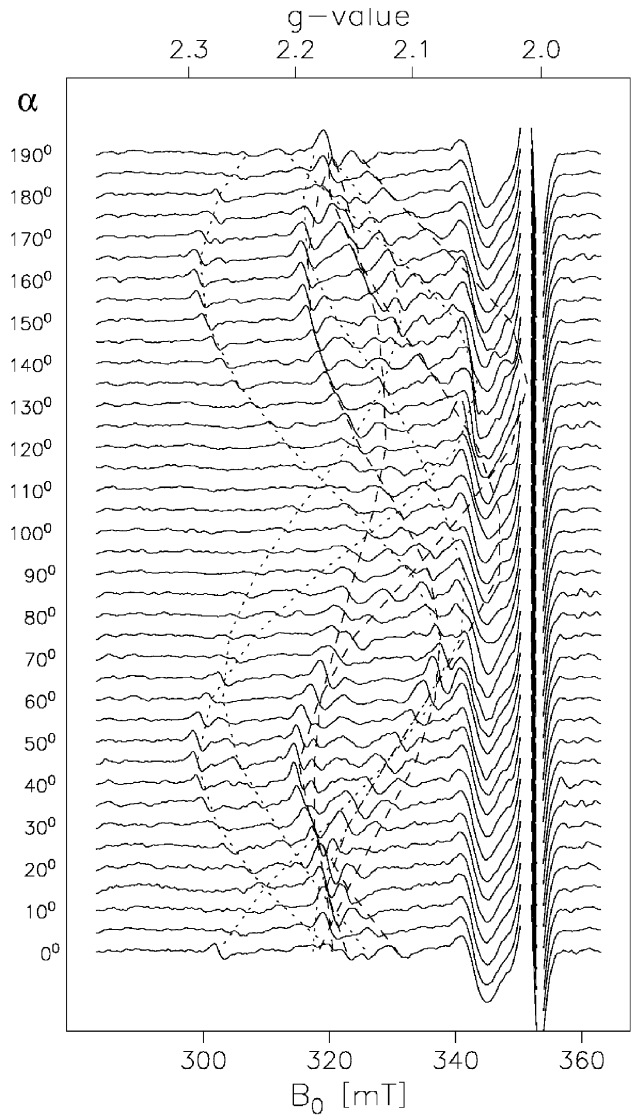

Figure 4. Angular dependence of EPR resonance positions of the reduced and illuminated [NiFe] cluster in a single crystal of [NiFe] hydrogenase from *D. vulgaris* Miyazaki F containing both Ni−C (•••) and Ni−L (- - -). Rotation of the sample in an arbitrary orientation about an angle α perpendicular to the applied magnetic field. The dominant signal at $g \approx 2.00$ results from reduced methyl viologen; at $g \approx 2.06$, a signal of the dielectric ring resonator due to Cr^{3+} impurities is observed that shows no angular dependence. Experimental conditions: X-Band, 9.8 GHz, $T = 50$ K, microwave power 1 mW, field modulation 100 kHz, modulation amplitude 1 mT, accumulation time 140 min for each trace.

metal centers and 0.24 Å for the main chain atoms.[13] In the active site, the Ni−S(Cys) bond angles were changed by less than 7° and the respective bond lengths varied by ≤0.08 Å compared with those of the structure of the oxidized state.

The EPR spectra of oxidized (data not shown) and reduced single crystals exhibited resonance lines that varied systematically with the orientation of the crystal relative to B_0. According to the space group $P2_12_12_1$, the periodicity of the angular dependent spectra is 180°. In the case of oxidized single crystals, the spectra exhibited two sets of four lines that correspond to the presence of the two paramagnetic species, Ni−B and Ni−A. In the oxidized enzyme, ratios of EPR active species of about 70 ± 10% Ni−B and 30 ± 10% Ni−A were found both in the protein solution and in the single crystals.[33,34] Upon reduction of the solution with hydrogen, we typically obtained a spin

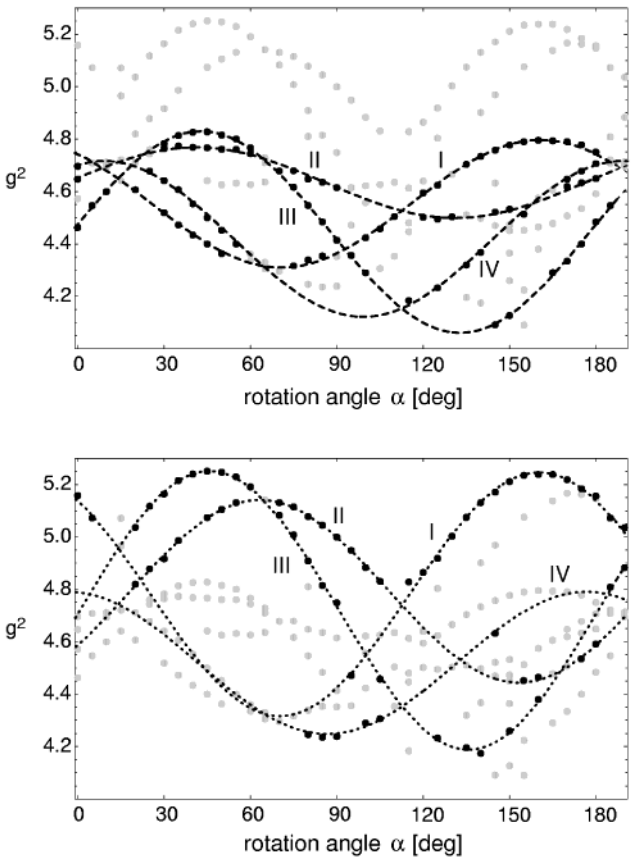

Figure 5. Angular dependence of the effective g^2 values. The dots represent experimental values derived from the spectra depicted in Figure 4. The black dots (●) are the values taken for the fit routine. The curves show the theoretical resonance positions for Ni−C (- - -, top) and Ni−L (•••, bottom) calculated by a simultaneous fit of all four sites to the resonances of the respective state.[33] The four sites per unit cell are marked by roman numbers. A 180° rotation of the *g* tensor orientation of site I about the crystal axis *a* yields site II, about *b* yields site III, and about *c* yields site IV, respectively. Note that a relation between the site numbering of Ni−C and Ni−L cannot be given a priori (see text).

concentration of 40 ± 10% relative to that observed in the oxidized state (Ni−A/Ni−B), in agreement with values found in the literature.[50] It can be assumed that the rest is in the EPR silent state (Ni−Si).[2] Under hydrogen gas atmosphere, the Ni−A/Ni−B signals in the single crystals vanished completely and a new species, Ni−C, appeared. Only one set of four resonance lines at maximum was observed in the spectra (data not shown) which indicated the presence of one paramagnetic species in the reduced single crystal. By illuminating the crystal at low temperatures, an additional set of resonance lines, which could be assigned to the Ni−L species, was generated (see Figure 4).

The effective *g* values of the EPR transitions $g_j(\theta,\phi)$ were directly taken from the EPR spectra (error: $\Delta\alpha \approx \pm 1°$, $\Delta g \pm 0.002$). Because of the strong superimposed EPR signal of methyl viologen at $g \approx 2.00$, we only considered the range of $2.291 \geq g_j(\theta,\phi) \geq 2.033$ in our analysis. The results of the fits for Ni−C and for Ni−L are shown in Figure 5.

The fit procedure yielded the principal *g* values and the direction cosines of the *g* tensor principal axes with respect to the crystal frame (Table 1). The *g* tensor principal values determined from the analysis of single crystal EPR spectra were

(50) Coremans, J. M. C. C.; van der Zwaan, J. W.; Albracht, S. P. J. *Biochim. Biophys. Acta* **1992**, *1119*, 157−168.

Table 1. Principal Values and Direction Cosines of the *g* Tensors of Ni−C and Ni−L in Single Crystals of the [NiFe] Hydrogenase from *D. vulgaris* Miyazaki F[a]

Ni−C

	1	2	3
g_i	2.198	2.142	2.012
l_{ai}	0.461	0.455	−0.762
l_{bi}	−0.204	−0.781	−0.590
l_{ci}	−0.864	0.428	−0.267

Ni−L

	1	2	3
g_i	2.298	2.116	2.045
l_{ai}	0.556	0.355	−0.751
l_{bi}	−0.325	−0.739	−0.590
l_{ci}	−0.765	0.572	−0.296

[a] g_i: *g* tensor principal values ($i = 1, 2, 3$) as obtained from the fit routine. l_{ki}: direction cosines of the *g* tensor principal axes ($i = 1, 2, 3$) in the crystal axes system ($k = a, b, c$) for the respective sites I of the four magnetically inequivalent sites.

identical within error to the values for Ni−C and Ni−L in frozen solutions (Table 1). The error of the *g* tensor orientations was determined to be less than 2°. According to the space group $P2_12_12_1$, four different *g* tensor orientations were obtained. The direction cosines of the principal axes of the *g* tensor of the remaining three sites can be obtained by appropriate rotations about one crystal axis (*a*, *b*, or *c*), which corresponds mathematically to a permutation of signs. This has been done independently for Ni−C and Ni−L.

Experimental *g* Tensor Orientation of the Ni−C State. In the next step, the *g* tensor axes in the crystal frame had to be assigned to the four possible sites in the unit cell. In principle, this is not possible from the EPR data alone. However, when the four possible assignments are compared, one assignment is favored on the basis of molecular orbital and crystal field theory considerations as detailed later. The four possible *g* tensor orientations of the Ni−C state of the active site of the hydrogenase from *D. vulgaris* Miyazaki F are overlayed to the X-ray structure of the reduced enzyme[13] in Figure 6. Since the largest part of the spin density of the [NiFe] cluster is located at the Ni atom[20−22] and the nickel ion contributes most to the *g* anisotropy (via its dominant spin−orbit coupling[51]), the displayed *g* tensors are centered on this atom.

The spatial structure of the catalytic center and the *g* tensor orientations are closely related to each other, since the interaction of the unpaired electron spin at the metal site with the surrounding ligands largely determines the orientation of the axes.[32] In the oxidized forms, the coordination of the Ni atom in the active site can be described either as a slightly distorted octahedron where one ligand position is empty or as a strongly distorted square pyramid (Figure 1). Upon reduction, the bridging ligand is removed (Figure 1) and supposedly replaced by a hydrogenic species; thus, a coordination sphere similar to Ni−A/B should be retained (see later). EXAFS studies indicated that the formal oxidation state of the Ni center is Ni(III) in Ni−A, Ni−B, and Ni−C.[52] The g_3 values in all these states are close to the free electron value g_e, and the other principal *g*

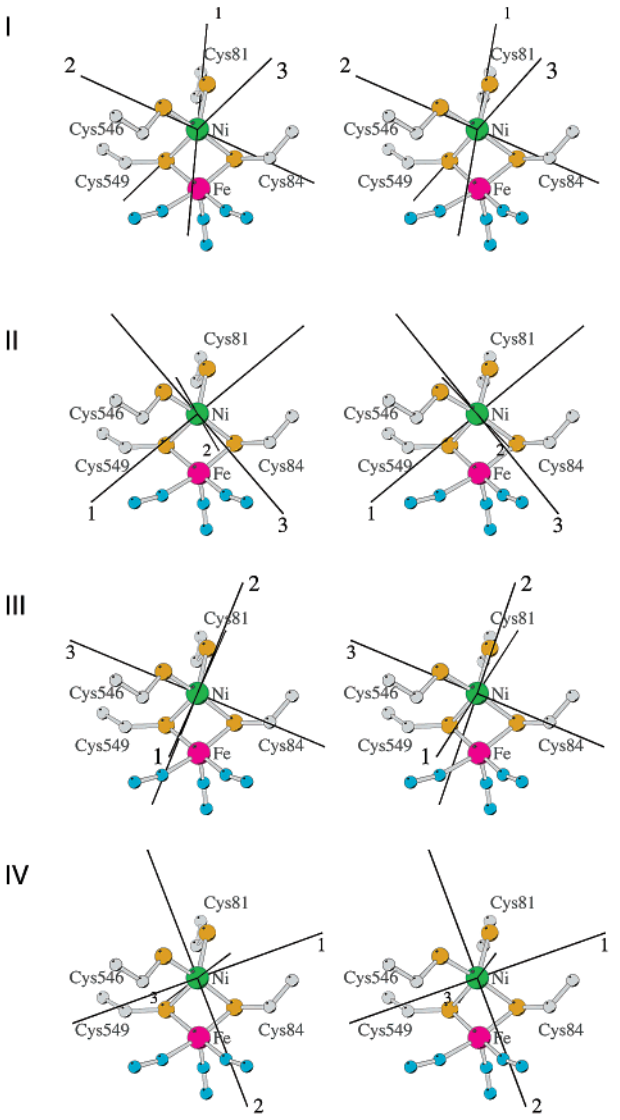

Figure 6. Stereoviews of the four possible *g* tensor orientations of Ni−C obtained from analysis of the single crystal EPR spectra of the reduced enzyme. The roman numbers correspond to the labeling of the four sites as indicated in Figure 5, top.

values are notably larger than 2. This indicates a formal Ni(III) in a $3d^1_{z^2}$ ground state in all three cases,[32] which is also supported by the results of DFT calculations[25] as discussed later. When the coordination geometry and the nature of the ground state of the active state are taken into account, the directions of the g_3 axis should be retained in all these states, that is, along the Ni−S(Cys549) bond and pointing to the unoccupied sixth coordination site in the X-ray structure (Figure 1).

We calculated the angles between the *g* tensor principal axes and the respective Ni−S bonds of the coordinating cysteines for all four possibilities using the coordinates of the X-ray structure of the reduced enzyme[13] (Table 2). Only one out of the four given orientations fulfilled the above-discussed criterion, as all other orientations notably deviate from the Ni−S(Cys549) bond (see Figure 6).

The following assignment of the *g* tensor axes for the Ni−C state is therefore proposed: The g_3 direction is retained with respect to the oxidized states, and it deviates only by an angle of 7° from the g_3 axis of Ni−B;[34] g_1 and g_2 are exchanged with respect to the oxidized states Ni−A and Ni−B. The g_3 axis of

(51) Salerno, J. C. In *Bioinorganic chemistry of nickel*. Lancaster, J. R., Jr., Ed.; VCH: New York and VCH Verlagsgesellschaft mbH: Weinheim, Germany, 1988; Chapter 3, pp 53−71.
(52) Davidson, G.; Choudhury, S. B.; Gu, Z.; Bose, K.; Roseboom, W.; Albracht, S. P. J.; Maroney, M. J. *Biochemistry* **2000**, *39*, 7468−7479.

Table 2. Angles (deg) between the Ni−S(Cys) Bonds of the X-ray Structure of the Reduced Hydrogenase from *D. vulgaris* Miyazaki F^{13} and the g_i Tensor Principal Axes ($i = 1, 2, 3$) of the Ni−C and the Ni−L States for the Four Different Sites

		Ni–C			Ni–L		
site	direction	1	2	3	1	2	3
I	Ni−S(Cys81)	**12**	90	78	**17**	80	76
	Ni−S(Cys84)	87	**14**	76	77	**19**	77
	Ni−S(Cys546)	84	**17**	74	86	**15**	75
	Ni−S(Cys549)	85	88	**5**	87	88	**3**
II	Ni−S(Cys81)	45	74	49	51	68	48
	Ni−S(Cys84)	78	45	48	84	42	48
	Ni−S(Cys546)	74	38	57	82	33	58
	Ni−S(Cys549)	41	50	83	30	61	84
III	Ni−S(Cys81)	32	60	80	42	49	82
	Ni−S(Cys84)	72	63	33	69	67	32
	Ni−S(Cys546)	62	65	39	59	70	38
	Ni−S(Cys549)	81	20	72	71	27	72
IV	Ni−S(Cys81)	54	40	74	65	31	73
	Ni−S(Cys84)	55	45	66	47	53	66
	Ni−S(Cys546)	51	54	60	44	62	59
	Ni−S(Cys549)	58	74	36	61	68	38

Ni−C deviates from the Ni−S(Cys549) bond by an angle of only 5°; g_1 lies near the Ni−S(Cys81) bond. The orientation of the g_2 axis corresponds approximately to the S(Cys546)−Ni−S(Cys84) direction (see site I in Figure 6).

Our proposed *g* tensor orientation is supported by the following experiments: (i) Guigliarelli et al. analyzed the solution EPR spectra of "split" Ni−C of the hydrogenase from *D. gigas* recorded at different microwave frequencies.[19] When the principal *g* values of the proximal $[4Fe-4S]^+$ cluster are assumed to be similar to those of $[4Fe-4S]^+$ ferredoxins, the EPR spectra have been simulated by considering the magnetic interactions between two point dipoles, namely the [NiFe] center and the proximal iron−sulfur cluster. The relative arrangement and *g* tensor orientation of the Ni center with respect to the proximal cluster were obtained. The resulting *g* tensor orientation is similar to the one we determined for the oxidized states, Ni−A and Ni−B,[34] which have the g_3 axis in the same direction as the reduced states. (ii) Orientationally selected ENDOR spectroscopy was performed recently on the Ni−C state in a related [NiFe] hydrogenase.[53−55] The ENDOR spectra were analyzed in detail and could only be simulated satisfactorily by using our proposed *g* tensor orientation (site I).[54,55]

Müller et al.[35] published a *g* tensor orientation for Ni−C derived from the analysis of orientationally selected ENDOR spectra of the [NiFe] hydrogenase from *D. gigas* and the [NiFeSe] hydrogenase from *D. baculatum*, both measured in frozen solution. They performed a simultaneous fit of the proton hyperfine couplings at the respective positions, the *g* tensor orientation, and the spin density distribution to the ENDOR data. The proposed *g* tensor orientation by the authors significantly deviates from all four possible *g* tensor orientations obtained by our single crystal EPR studies and can therefore not be correct.

Table 3. Comparison of Calculated *g* Tensor Principal Values for Various Complexes with Different Types of the Bridging Ligand X between Ni and Fe with Experimental Values of Ni−C and Ni−L

oxidation state	type of bridge	g_1	g_2	g_3
Ni(III)	vacant bridge	2.28	2.03	1.99
Ni(III)	H^- axial,[a] vacant bridge	2.13	2.06	2.02
Ni(III)	H^+ axial,[a] H^- bridge	2.13	2.02	1.96
Ni(III)	H^+−S(Cys546), H^- bridge	2.24	2.06	1.99
Ni(III)	H^- bridge	2.20	2.10	2.00
Ni(I)	vacant bridge	2.26	2.10	2.05
Ni(I)	H^- bridge	2.09	2.03	2.03
Ni−C (expt)		2.20[b]	2.14	2.01
Ni−L (expt)		2.30	2.12	2.05

[a] Ligand bound to Ni at the sixth position (see arrow in Figure 2). [b] In ref 2, a value of 2.19 was found.

DFT Calculations of the *g* Tensor Orientation in Ni−C. In the crystal structure of the reduced form, the bridging ligand found in the oxidized forms Ni−A and Ni−B[15,8] is removed and its position is vacant.[56,13] EPR spectroscopy cannot detect a potential substrate (H_2) or product (H^+ or H^-) binding in this site, since the hyperfine interaction is smaller than the EPR line width. ENDOR investigations of the Ni−C state of [NiFe] hydrogenases were performed, in both H_2O and D_2O, on [NiFe] hydrogenases from *Thiocapsa (Th.) roseopersicina*[57] and from *D. gigas*[58] and found large D_2O exchangeable hyperfine couplings of about A(H1) ≈ 17 and 20 MHz, respectively. It was proposed that this coupling belongs to a hydrogenic species directly bound to the Ni center, probably in an in-plane position relative to the $3d_{z^2}$ orbital.[58] This result was considered in finding an appropriate structural model for the catalytic site in the Ni−C state for our DFT calculations.

First, we have calculated a formal Ni(III) oxidation state with a vacant bridging position, with a bridging proton, with an axially coordinated H^-, and with an axial H^+. Neither yielded *g* values in good agreement with experiment (Table 3). A formal Ni(I) oxidation state with an empty bridge or a bridging hydride could also not reproduce the experimental results. The involvement of the ligating cysteine residues in the hydrogen cleavage has also been tested. Protonation of a bridging cysteine led to a breakup of coordination to one metal ion.[59] Therefore, a proton at one of these sulfur atoms could be excluded. The terminal cysteines may however act as base in the heterolytic hydrogen cleavage process. Assuming that the hydride remains in the position of the bridging ligand and, for example, Cys546 is protonated in the Ni−C state, one obtains *g* values that do not agree well with experimental data (see Table 3). Only when an Ni(III) with an H^- bridge located between Ni and Fe was used, good agreement with the *g* tensor magnitudes *and* the principal axes orientation has been obtained. The calculated *g* tensor orientation shows that g_3 is indeed retained compared to the direction in Ni−A/B; it lies close to the Ni−S(Cys549) bond. The g_1 and g_2 axes are approximately interchanged compared to the oxidized forms; in the Ni−C state, the g_1 axis with the largest principal *g* value points toward the position of the

(53) Ni−C was studied in the regulatory [NiFe] hydrogenase from *Ralstonia (R.) eutropha* that shows EPR[54,55] and FTIR[64,67,68] signals typical for the Ni−C state in standard hydrogenases and is thus a good model for this system.[54]
(54) Brecht, M. *Hochfeld und Puls EPR Untersuchungen an den Kofaktoren von [NiFe]-Hydrogenasen: Beiträge zur Klärung des Mechanismus der biologischen Wasserstoffspaltung*. Doctoral Thesis, Technische Universität Berlin, Berlin, Germany, 2001.
(55) Buhrke, T.; Brecht, M.; Lubitz, W.; Friedrich, B. *J. Biol. Inorg. Chem.* **2002**, *7*, 897−908.
(56) Garcin, E.; Vernede, X.; Hatchikian, E. C.; Volbeda, A.; Frey, M.; Fontecilla-Camps, J. C. *Structure* **1999**, *7*, 557−566.
(57) Whitehead, J. P.; Gurbiel, R. J.; Bagyinka, C.; Hoffman, B. M.; Maroney, M. J. *J. Am. Chem. Soc.* **1993**, *115*, 5629−5635.
(58) Fan, C.; Teixeira, M.; Moura, J.; Moura, I.; Huynh, B. H.; LeGall, J.; Peck, H. D., Jr.; Hoffman, B. M. *J. Am. Chem. Soc.* **1991**, *113*, 20−24.
(59) Pavlov, M.; Siegbahn, P. E. M.; Blomberg, M. R. A.; Crabtree, R. H. *J. Am. Chem. Soc.* **1998**, *120*, 548−555.

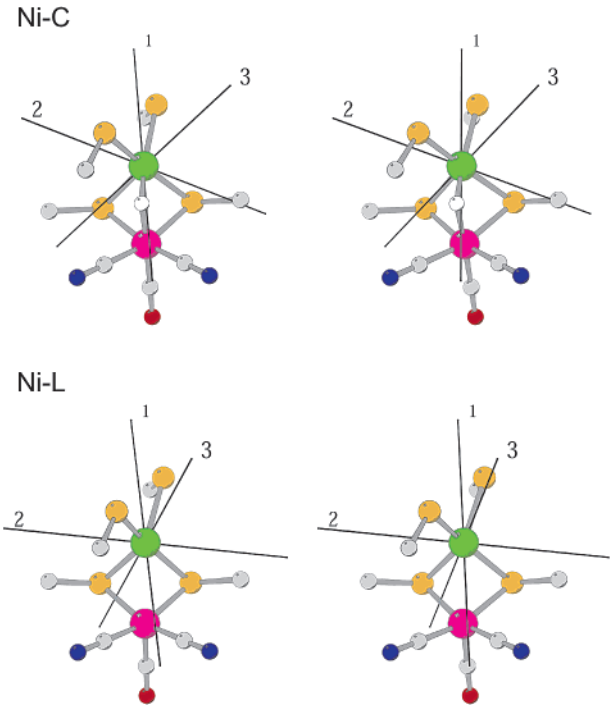

Figure 7. Stereoviews of the resulting *g* tensor orientations of Ni−C and Ni−L obtained from DFT calculations on the geometrically optimized structures shown. Note that the Cys residues are truncated for clarity.

(bridging) hydride (see Figure 7). The calculated *g* tensor orientation compares remarkably well with the experimentally determined site I. The calculated angle is 15° between g_1 and Cys81, 12° between g_2 and Cys84, and 4° between g_3 and Cys549. The respective experimental angles (site I) are 12°, 14°, and 5° (see Table 2). The other three possible experimental orientations, belonging to the other three sites, do *not* agree with the calculations.

We subsequently took a closer look at the electronic structure of the Ni atom in the Ni−C form. A natural atomic charge (NAC) analysis yielded an orbital occupation of the unpaired electron of $3d_{xy}^{0.02}$, $3d_{xz}^{0.06}$, $3d_{yz}^{-0.05}$,$3d_{x^2-y^2}^{0.09}$, and $3d_{z^2}^{0.48}$ and thus showed the clear preference of the $3d_{z^2}$ orbital. The remaining spin density is delocalized over the sulfur atoms of the coordinating cysteine amino acid residues (see ref 25). It should be mentioned that we also obtained good agreement between the calculated and available experimental ^{1}H, ^{57}Fe, and ^{61}Ni hyperfine coupling constants for Ni−C in the chosen geometry.[29] This agreement of the *g* tensor principal magnitudes and orientations and the hfc's of various magnetic nuclei indicates that the structure of the Ni−C intermediate is basically correct.

Experimental *g* Tensor Orientation of the Ni−L State. The set of direction cosines for Ni−L derived from the fit routine is very similar to that of Ni−C (see Table 1). However, the assignment to the four molecules in the unit cell for Ni−C and Ni−L is a priori not known. A possible assumption is that the orientation is not significantly changed in the light-induced process at low temperatures (although the *g* tensor magnitudes are). On the basis of this model, we looked for the most similar axes orientations. The result is shown in Figure 8 in which both experimental *g* tensors of Ni−C and Ni−L are assigned to site I. In this assignment, the g_3 axis is retained in both states (deviation of 2°), whereas those of g_1 and g_2 are rotated in plane by 10°.

An indication that the *g* tensor orientations of Ni−C and Ni−L are similar comes from studies of Dole et al.[60] These authors analyzed the "split" Ni−C and Ni−L EPR spectra in frozen solutions of the standard hydrogenase from *D. gigas*[60] which result from the magnetic interaction with the proximal $[4Fe-4S]^+$ cluster ($S = {}^1/_2$). It was found that the relative orientations of the magnetic axes of the proximal Fe−S cluster and the [NiFe] center in the Ni−L state and the Ni−C state are not greatly changed by the photodissociation process. The deviations between the *g* tensor axes of the two investigated states were found to be relatively small (25° for g_3).[60] It can be assumed that the electronic structure and the *g* tensor orientation of the iron sulfur cluster are not affected by the illumination.

Comparing the EPR spectra of hydrogenase in the different paramagnetic states, one finds that Ni−L no longer exhibits a resonance line near $g \approx 2.0$ as Ni−A, Ni−B, and Ni−C. The lowest *g* value is now shifted to $g \approx 2.05$. It has been proposed that this finding indicates a ground state different from $3d_{z^2}^1$ and a formal $3d_{x^2-y^2}^1$ ground state has been discussed for this situation (see ref 32 and references herein). If we assume a $3d_{x^2-y^2}^1$ ground state, the *g* tensor axes should not deviate much from the Ni−S(cysteine) bonds, the same holds if the $3d_{z^2}^1$ ground state is retained. In Table 2, the deviation of the Ni−L *g* tensor axes from the Ni−S(Cys) ligand bond directions are given for the four different sites in the crystal unit cell. Only one out of four possible orientations, namely site I, which is very similar to the *g* tensor orientation of Ni−C, fulfilled the requirement of minimal deviations between the *g* tensor axes and the Ni−S(Cys) bonds. The same assignment has been found as the most likely one in the case of Ni−C (see above), showing that the two *g* tensor orientations are indeed very similar.

For the Ni−C state, we have shown that this species is best described by an Ni(III) bearing a hydride bridge (H^-) between the nickel and the iron atom. Earlier EPR and ENDOR experiments[57] on standard hydrogenase conclusively showed a large exchangeable proton hyperfine coupling that was lost upon conversion of Ni−C to Ni−L. This effect was interpreted as a photodissociation of a hydrogenic species bound to the EPR active center[54,58,57,61] that probably leads to a redistribution or an increase of the electron density at the [NiFe] site, as detected by IR spectroscopy.[11,62] XAS data do not show a pronounced Ni K-edge shift upon conversion from Ni−C to Ni−L that would indicate a metal centered two electron photoreduction process at the [NiFe] site.[52,57] Also, a change in the number of ligands at the nickel site could not be detected by means of EXAFS; however, the determination of the absolute number of ligands is quite difficult, especially in the case of hydrogen being a possible candidate.[52,57] We assume that in this dissociation process the bridging hydrogen is lost, either as H^- or as H^+, the latter leading to a formal reduction of the [NiFe] site in the Ni−L state. In this limited valence picture, one would obtain a formal Ni(III) d^7 or a formal Ni(I) d^9 species, respectively. This question can be solved by a comparison of the experimental *g* tensor magnitudes and orientations with those calculated by DFT on various structural models of the active site as detailed below.

(60) Dole, F.; Medina, M.; More, C.; Cammack, R.; Bertrand, P.; Guigliarelli, B. *Biochemistry* **1996**, *35*, 16399−406.
(61) van der Zwaan, J. W.; Albracht, S. P. J.; Fontijn, R. D.; Slater, E. C. *FEBS Lett.* **1985**, *179*, 271−277.
(62) Bagley, K.; Duin, E. C.; Roseboom, W.; Albracht, S. P. J.; Woodruff, W. H. *Biochemistry* **1995**, *34*, 5527−5535.

Table 4. Comparison of Calculated and Experimental *g* Tensor Principal Values and Orientations of Ni−L. Deviations of the *g* Tensor Axes Orientation from the Nickel−Ligand Bonds Are Given in Degrees

		g values			*g* tensor axes orientation		
		g_1	g_2	g_3	∠ (g_1–S(Cys81))	∠ (g_2–S(Cys84))	∠ (g_3–S(Cys549))
Ni−L[a]	ZORA[c]	2.276	2.101	2.054	17	49	37
Ni−L[b]	ZORA[c]	2.257	2.097	2.049	22	34	23
Ni−L[b]	QR ROKS[d]	2.291	2.112	2.067	24	18	15
Ni−L[b]	QR UKS[d]	2.211	2.138	2.090	22	13	8
Ni−L (expt)	site I	2.298	2.116	2.045	17	19	3

[a] Geometry of Ni−C retained for this calculation. [b] Optimized geometries of Ni−L used for *g* tensor calculations. [c] ZORA denotes the "zero-order regular approximation" Hamiltonian[28] which treats spin−orbit coupling self-consistently. [d] QR is the "quasi-relativistic" Hamiltonian[65] which allows a spin-restricted (ROKS) and spin-unrestricted (UKS) approximate treatment of spin−orbit coupling.

DFT Calculations of the *g* Tensor Orientation in Ni−L. On the basis of the structural model of the Ni−L state developed in the previous section, we have performed relativistic DFT calculations to accurately describe the electronic structure of this species and to obtain the related *g* (and hyperfine) tensors (cf. also refs 16 and 29).

The following reactions are in principle possible. (i) Photodissociation of a hydride: The hydride is removed from Ni(III) and takes its two electrons with it.

$$\text{Ni(III)}-\text{C} \xrightarrow[-\text{H}^-]{h\nu} \text{Ni(III)}-\text{L}$$

Here, the Ni would remain in a formal Ni(III) state but a nearby hydride acceptor would have to be found. The calculation yields *g* values of 2.28, 2.03, and 1.99 (Table 3), which do not agree with the *g* values measured for the enzyme. (ii) The bridging ligand is removed as a proton: The two electrons remain at the nickel atom and formally reduce the metal from an Ni(III) in Ni−C to an Ni(I) in Ni−L.

$$\text{Ni(III)}-\text{C} \xrightarrow[-\text{H}^+]{h\nu} \text{Ni(I)}-\text{L}$$

The proton is transferred to a nearby acceptor, probably a basic amino acid like arginine. This leads to *g* values of 2.26, 2.10, and 2.05 (Table 3), which are in remarkably good agreement with the experimental values. In particular, the shift of g_3 to a value significantly different from g_e is reproduced. Thus, a loss of a proton and a change of the ground state in Ni−L are very plausible. The calculated *g* tensor orientation is similar to that obtained for the Ni−C form (see later).

Since the Ni−L state is generated by the illumination of Ni−C at low temperatures (<100 K), it remains to be seen whether the protein environment is going to relax to the energetic minimum at such low temperatures or whether it will be frozen in the Ni−C conformation. Evidence for conformational changes comes from the fact that in [NiFe] hydrogenases at least two different Ni−L states can be observed.[54,63,64] When the model cluster is geometrically optimized upon removal of the bridging ligand, the Ni−Fe distance elongates from 2.62 Å in the Ni−C form to 2.71 Å. The calculated *g* tensor principal values sligthly decrease upon relaxation of the active site structure (see Table 4). The overall orientation of the *g* tensor principal axes is retained, but in the relaxed structure, the principal axes are somewhat more closely oriented along the Ni−ligand bonds.

The deviation between the measured and calculated *g* tensor orientations for Ni−L (see Table 4) is larger than that for the Ni−C form. This may be due to the fact that the photodissociated proton, which is probably transferred to a nearby amino acid, has not been included in our calculations. Nevertheless, we can reproduce the overall experimental *g* tensor orientation (see Figure 7). From the calculations alone, a definite conclusion about the structural parameters of the active site upon illumination cannot be made. The electronic structure is not greatly affected by relaxing the structural constraint of the Ni−C conformation.

In the ZORA Hamiltonian, the spin−orbit coupling is treated variationally in a self-consistent spin-restricted manner. We have also performed spin-unrestricted *g* tensor calculations in which the spin−orbit coupling is treated perturbationally in a quasi-relativistic (QR, Pauli Hamiltonian) calculation.[65] The same functional, basis set and integration scheme were used. Because of the perturbative treatment of spin−orbit coupling, the obtained *g* tensor principal values are more erroneous than those obtained from the ZORA Hamiltonian (see Table 4). One can show that the effect of spin polarization significantly influences both the *g* tensor principal values and the orientation by comparing spin-restricted (ROKS) and spin-unrestricted (UKS) calculations. When spin polarization is considered, one obtains a better agreement with the experimental site I for the *g* tensor orientation in Ni−L (see Table 4).

In the Ni−L state, the NAC analysis yields: $3d_{xy}^{0.01}$, $3d_{xz}^{0.02}$, $3d_{yz}^{0.01}$, $3d_{x^2-y^2}^{0.26}$, and $3d_{z^2}^{0.64}$. The total unpaired spin density at the nickel nucleus increases. This is in agreement with experimental observations of the ^{61}Ni hyperfine splitting in the Ni−C and Ni−L forms.[66] The relative weight of the $3d_{x^2-y^2}$ orbital compared to that of the $3d_{z^2}$ orbital increased from 20% in Ni−C to 40% in Ni−L. But still there is a predominant preference of the $3d_{z^2}$ orbital in this analysis which explains a *g* tensor orientation of the Ni−L state similar to the Ni−C state and supports our assignment to site I.

(63) van der Zwaan, J. W.; Albracht, S. P.; Fontijn, R. D.; Mul, P. *Eur. J. Biochem.* **1987**, *169*, 377−384.
(64) Pierik, A. J.; Schmelz, M.; Lenz, O.; Friedrich, B.; Albracht, S. P. J. *FEBS Lett.* **1998**, *438*, 231−235.
(65) Schreckenbach, G.; Ziegler, T. *J. Phys. Chem. A* **1997**, *101*, 3388−3399.
(66) Foerster, S. *EPR spectroscopic investigation of the active site of [NiFe]-Hydrogenase: A contribution to the elucidation of the reaction mechanism.* Doctoral Thesis, Technische Universität Berlin, Berlin, Germany, 2003.
(67) Pierik, A. J.; Roseboom, W.; Happe, R. P.; Bagley, K. A.; Albracht, S. P. J. *J. Biol. Chem.* **1999**, *274*, 3331−3337.
(68) Kleihues, L.; Lenz, O.; Bernhard, M.; Buhrke, T.; Friedrich, B. *J. Bacteriol.* **2000**, *182*, 2716−2724.
(69) Kraulis, P. J. *J. Appl. Crystallogr.* **1991**, *24*, 946−950.
(70) Fahnenschmidt M. *De novo synthetisierte Proteine mit Metalloporphyrinkofaktoren*. Doctoral Thesis, Technische Universität Berlin, Berlin, Germany, 2000.

Conclusion and Outlook

In this work, the active state Ni−C in the reaction cycle of [NiFe] hydrogenase and the related light induced Ni−L state have been studied by EPR at low temperatures for the first time in reduced and illuminated hydrogenase single crystals from *D. vulgaris* Miyazaki F. This allowed a precise determination not only of the *g* tensor magnitudes but also of the *g* tensor axes orientations with respect to the crystal axes. On the basis of various experimental and theoretical results, a plausible assignment of the *g* tensors to a specific site and thus to the atomic structure of the active NiFe center could be achieved for both Ni−C and Ni−L. The axes are compared to those obtained earlier[34] for the oxidized states Ni−A and Ni−B in Figure 8.

For the reduced Ni−C as well as for the oxidized states Ni−A and Ni−B,[34] a formal Ni(III) in a $3d^1_{z^2}$ electronic configuration is proposed and for all three states a similar *g* tensor orientation is obtained. The g_3 axis is almost parallel to the Ni−S(Cys549) bond. However, in the Ni−C state, an exchange of the g_1 and g_2 axes occurred with respect to Ni−A and Ni−B. Apparently, the exchange of the bridging oxygenic (O^{2-}/OH^-; see ref 7) or sulfuric (S^{2-}/SH^-; see refs 8 and 13) ligand for a hydrogenic species (H^-, H^+, or H_2; see ref 13) does not change its preferred direction but leads to a difference in the *g* tensor magnitudes and the spin density distribution. In the Ni−L state, experiments indicate a formal Ni(I) redox state, which is obtained via reversible photodissociation of a proton from the bridging position. A *g* tensor orientation resembling the orientation in the Ni−C state was determined, although the *g* tensor magnitudes are quite different.

The experimental results have been compared with relativistic DFT calculations within the ZORA approximation performed on geometrically optimized model structures for the active site of the [NiFe] hydrogenase. In these calculations, the oxidation state of the nickel (either formal Ni(I) or Ni(III) oxidation states), the type of the third bridging ligand X between nickel and iron, and possible protonation sites have been varied. The limited-size models used are already able to reproduce well the experimentally observed *g* tensors. A good agreement between experimental and calculated magnitudes and orientations of magnetic resonance parameters was obtained when a formal Ni(III) state with a hydride (H^-) bridge was chosen for Ni−C and a formal Ni(I) with a vacant bridge was chosen for Ni−L. The detailed analysis of DFT calculations showed that in both states the majority of unpaired spin density is at the nickel (51% and 76% for Ni−C and Ni−L, respectively[29]) and only a small amount is at the Fe. However, a considerable fraction of the unpaired spin density is found at the sulfur ligands (see ref 25). A natural atomic charge (NAC) analysis shows that Ni−C is correctly described by a $3d_{z^2}$ ground state, whereas in Ni−L a substantial fraction of the unpaired electron is additionally found in the $3d_{x^2-y^2}$ orbital. This explains the experimentally observed difference of the *g* tensor values.

On the basis of the described experimental and theoretical results, a picture of the electronic and geometrical structure and composition of the Ni−C and the related Ni−L states arises that contributes to understanding the detailed mechanism of hydrogen conversion by the enzyme [NiFe] hydrogenase. Recently, we could show by ENDOR and ESEEM experiments

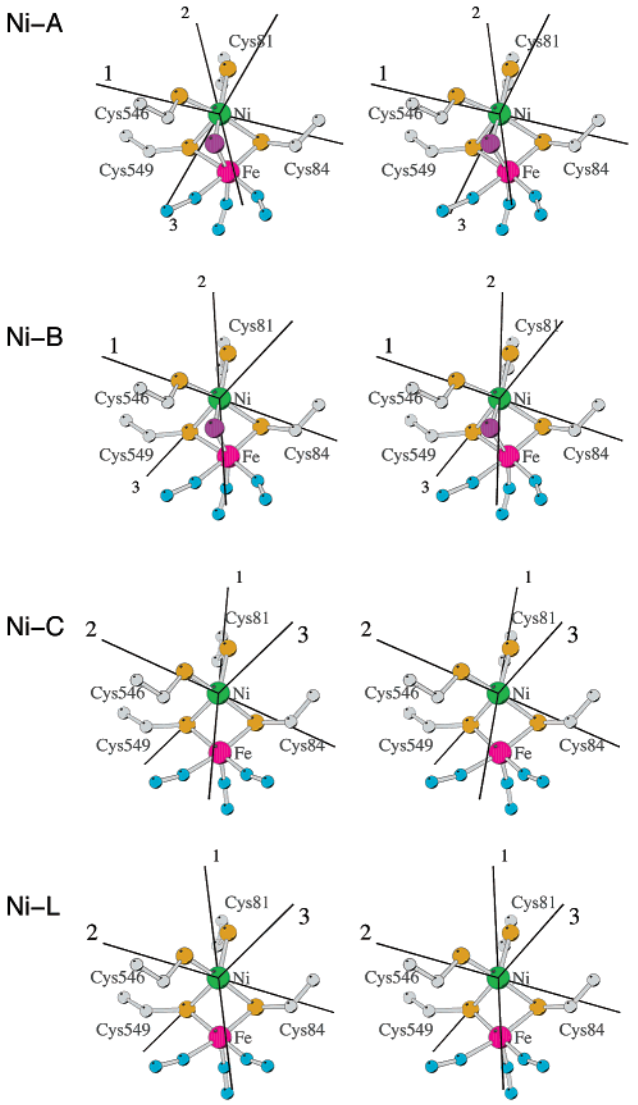

Figure 8. Overview over the *g* tensor orientations as determined from EPR studies of single crystals of the hydrogenase from *D. vulgaris* Miyazaki F of the paramagnetic states Ni−A, Ni−B,[34,40] Ni−C, and Ni−L (this work). The *g* tensors are depicted in the respective X-ray crystallographic structures of the oxidized[8] and the reduced form.[13] In the latter, the bridging position is empty (see Figure 1).

performed on the Ni−C and Ni−L state that the proposal of a hydride bridge in Ni−C, which is lost upon illumination, is correct.[54] This shows that the hydrogen is cleaved heterolytically by the enzyme and the hydride is bound between the Ni and Fe. It is expected that the released proton is transferred in an intermediate step to a sulfur or oxygen (water) species near the active metal center and is subsequently released. The reversible photodissociation of the Ni−C state to form Ni−L, the temperature and wavelength dependence of this process, and the detailed mechanism of the postulated proton transfer to a nearby acceptor remain to be determined in the future.

Acknowledgment. This paper is dedicated to Prof. Dr. Karl Wieghardt on the occasion of his 60th birthday. We thank Dr. Olga Schröder and Dr. Maurice van Gastel for helpful discussions concerning the interpretation of the data. This work was supported by DFG (Lu 315/13 and Sfb 498, TP C2), COST action 841, Fonds der Chemischen Industrie (to W.L.), JSPS

KAKENHI (No. 1438017) and COE program, JBA, NEDO, METI, and National Project on Protein Structural and Functional Analyses.

Note Added in Proof

In a recent paper,[71] it was shown by ^{17}O ENDOR experiments that in the Ni−A state of *D. gigas* [NiFe] hydrogenase an oxygen bridge (O^{2-} or OH^-) is indeed present between Ni and Fe that is lost upon conversion to the Ni−C state.

JA027522U

(71) Carepo, M.; Tierney, D. L.; Brondino, C. D.; Yang, T. C.; Pamplona, A.; Telser, J.; Moura, I.; Moura, J. J. G.; Hoffman, B. M. *J. Am. Chem. Soc.* **2002**, *124*, 281−286.